



Urban growth of the Washington, D.C.–Baltimore, MD metropolitan region from 1984 to 2010 by annual, Landsat-based estimates of impervious cover

Joseph O. Sexton ^{a,*}, Xiao-Peng Song ^a, Chengquan Huang ^a, Saurabh Channan ^a,
Matthew E. Baker ^b, John R. Townshend ^a

^a Global Land Cover Facility, Department of Geographical Sciences, University of Maryland, 2181 LeFrak Hall, College Park, MD 20742, United States

^b Department of Geography and Environmental Systems, University of Maryland, Baltimore County, United States

ARTICLE INFO

Article history:

Received 13 April 2012

Received in revised form 19 October 2012

Accepted 27 October 2012

Available online xxx

Keywords:

Urbanization

Impervious surface

Land cover

Landsat

Washington, DC

Baltimore, MD

Chesapeake Bay

ABSTRACT

Cities and surrounding suburbs are Earth's fastest growing land use. Urban impervious surfaces affect hydrological and energy balances, as well as biological composition and functioning of ecosystems. Although datasets have been produced documenting urban growth at multiple time periods in coarse intervals, there remains an unmet need for observations spanning multiple decades at high frequency. We have developed an empirical method for retrieving annual, long-term continuous fields of impervious surface cover from the Landsat archive and applied it to the Washington, D.C.–Baltimore, MD megalopolis from 1984 to 2010. Fitting and applying a single regression model over time, the method relies on a multi-annual training sample of high-resolution impervious cover layers tied to coincident intra- and inter-annual Landsat image composites. These predictor images are composited and normalized to maximize discrimination of impervious surfaces from intermittently bare agricultural fields and minimize inter-annual variation due to phenology, solar illumination, and atmospheric noise. Excluding the year 2009 due to lack of data availability resulting from nearly continual winter snow cover, the resulting dataset is a continuous-field representation of impervious surface cover at 30-m horizontal and annual temporal resolution from 1984 to 2010. Average error was approximately $\pm 6\%$ cover, with outliers due to shadows from large buildings in winter images. The region's impervious surface cover grew from 881 to $1176 \pm 11 \text{ km}^2$ over the 27-year span—an average annual gain of approximately $11 \pm 2 \text{ km}^2/\text{year}$ —with great variability among local municipalities in terms of rate of development. Patterns including intensification (i.e., “infill”) and expansion (i.e., exurban or “sprawl”) of development, as well as fragmentation and isolation of natural areas were clearly visible in the data at various places and times. Neither impervious surface loss nor deceleration of growth were observed in any of the cities or counties over the study span. These findings show that empirical retrieval of impervious coverage at the spatial and temporal scale of the Landsat archive is possible using dense time-stacks of calibrated Landsat images, and that long-term records such as this can provide new opportunities for analyzing land-use patterns and their underlying causes to improve understanding of socio-economic processes and human–environment interactions.

© 2012 Elsevier Inc. All rights reserved.

1. Introduction

Although urban areas cover only 0.5% of Earth's terrestrial surface (Schneider et al., 2009), cities represent one of Earth's fastest growing land-use types on a per-area basis, and over half of the planet's 7 billion humans now reside in cities (UNFPA, United Nations Population Fund, 2011). A characteristic land cover and indicator of urban land use is impervious surface cover, a category grouping all surface materials through which precipitation does not penetrate, including paved roads, sidewalks, parking lots, buildings, and other built structures. Urban impervious surfaces generate the “urban stream syndrome” (Walsh et al., 2005), which is characterized by increased hydroperiod

variability, water temperature, sediment load, and levels of heavy metals, nitrogen, phosphorous, and fecal coliform bacteria. Urban surfaces also generate the “urban heat island effect” (Oke, 2006), an increase in temperature due to shifting energy balance toward sensible over latent heat fluxes that has been shown to alter regional climate, shift biotic community composition and even accelerate climate-induced species' range shifts (Menke et al., 2010). Urbanization is also associated with the “demographic transition” in humans (Davis, 1945), manifested by delayed reproduction and decreased birth and death rates leading to slower or even negative population growth rates.

Monitoring the spatio-temporal complexities of urbanization has been difficult. Land-use dynamics exhibit temporal nonlinearity and spatial heterogeneity due to complex interactions with the socio-economic and ecological environment (Lambin et al., 2003). Urbanization is a feedback system that is economically driven, promoted by

* Corresponding author. Tel.: +1 301 405 8165; fax: +1 301 314 9299.
E-mail address: jsexton@umd.edu (J.O. Sexton).

local zoning and taxation policies, and constrained by laws to conserve natural resources and open spaces (Westervelt et al., 2011). In order to monitor change and understand the causes and consequences of urbanization, land-cover datasets must have sufficient temporal resolution to record the complexities of change. Jensen and Cowen (1999) called for a 1- to 5-year basis for monitoring urbanization, similar to the recommendation of Lunetta et al. (2004) of a 3-year frequency for monitoring change in forests.

Impervious surfaces have been remotely sensed at a range of spatial scales using a variety of data sources and methods. Several global land cover datasets include urban categories (e.g., Friedl et al., 2002; Hansen et al., 2000; Loveland et al., 2000; Potere et al., 2009; Small et al., 2005), but the coarse resolution of such data sets is insufficient to represent spatial variation within cities, towns, and settlements. Using seasonal triplets of multi-spectral Landsat images, Yang et al. (2003) generated a percent impervious surface cover dataset for the 2001 United States' National Land Cover Dataset ("NLCD 2001") (Homer et al., 2004) at 30-m resolution. Leveraging the distinct geometric patterns of anthropogenic structures, high-resolution (<5 m) data have been used in manual digitization and automated image segmentation approaches to detecting impervious cover (e.g., Goetz et al., 2003; Thomas et al., 2003). Light Detection And Ranging (LiDAR) and Synthetic Aperture Radar (SAR) measurements of vertical structure are also increasingly being employed to detect urban and impervious types (Hodgson et al., 1999; Jiang et al., 2009).

Extension of impervious surface records into the temporal domain has been more difficult, and so the great majority of impervious surface datasets currently record only one point in time. However, multi-temporal remote sensing of urban cover has had some recent successes, and development is accelerating with recent increases in data availability. Masek et al. (2000) monitored urbanization around the Washington, D.C. metropolitan area in two broad intervals between 1973 and 1996 by subtracting NDVI images recorded by Landsat Multi-Spectral Scanner (MSS) and Thematic Mapper (TM) sensors. More recently, Yin et al. (2011) retrieved a time series of four maps between 1979 and 2009 from Landsat data to observe long-term acceleration in the development of the Shanghai metropolitan area, and Taubenböck et al. (2012) combined Landsat images from circa 1975, 1990, 2000, and 2010 and InSAR data from 2010 to monitor growth of 27 megacities at an approximately decadal interval. Suarez-Rubio et al. (2012) employed spectral endmember analysis, decision trees, and post-classification morphological analysis to assess exurban development near Washington, D.C. However, despite their advantages over static maps, bi-temporal, and even coarsely multi-temporal datasets do not have the necessary temporal scale to observe higher-order complexities (e.g., acceleration and deceleration) of land-cover and land-use change. In order to resolve these patterns, observations must span multiple decades at high frequency.

In this paper, we describe an empirical method for retrieving long-term records of impervious surface cover from time series of Landsat images, using the rapidly growing Washington, D.C.–Baltimore, MD metropolitan area as an exemplar of a variety of change dynamics. We estimate the uncertainty of our results by validation relative to an independent, withheld sub-sample of the reference data in multiple years. We then highlight characteristic patterns and dynamics of urbanization in the region, comparing our findings to previous studies in the region based on other methods.

2. Methods

2.1. Study area

Our study area was the path-15/row-33 scene of the Landsat World Reference System 2 (WRS-2), encompassing the Washington, D.C.–Baltimore metropolitan region on the eastern seaboard of the United States (Fig. 1). The natural vegetation of the region consists

predominantly of mixed forests dominated by deciduous tree species. Land use in the region is mainly agricultural, with many small towns and a few large urban agglomerations around the anchor cities of Washington, D.C. and Baltimore, Maryland. Although the region is among the nation's fastest-growing in terms of human population, most growth has been outside of urban cores. For example, while the human population of Washington shrank from 6.07×10^5 to 6.02×10^5 and that of Baltimore shrank from 7.36×10^5 to 6.21×10^5 residents between 1990 and 2010, three outlying Maryland counties—Calvert, Howard, and Montgomery—grew from 0.51×10^5 , 1.87×10^5 , and 7.57×10^5 residents in 1990 to 0.89×10^5 , 2.87×10^5 , and 9.72×10^5 residents in 2010 respectively (Maryland State Archives, 2011; US Census Bureau, 2012).

2.2. Model

We modeled impervious surface cover (ISC), the percentage of each pixel covered by impervious surfaces, as a piecewise-linear function of a set of predictors derived from multi-spectral measurements (X):

$$ISC_{i,t} = f(X_{i,t}),$$

where subscript i denotes the pixel's location in space and t refers to its location in time, indexed by year. By multiplying by the pixel's area (i.e., 900 m^2), ISC may be converted to impervious surface cover, ISA, expressed in areal units. Derivation of the spectral predictors, X , is described in the following section.

2.3. Data

Reference measurements of impervious cover were composed from vector GIS layers of impervious surfaces acquired from local jurisdictions over multiple years. Predictor data were seasonal composites of Landsat images. Between 1984 and 2010, every year was included in the analysis except 2009, which was excluded due to insufficient winter data availability resulting from record snowstorms and nearly continual winter snow cover.

2.3.1. Reference impervious data

Impervious surface data spanning multiple years were collected from planimetric data recorded by municipalities within the study

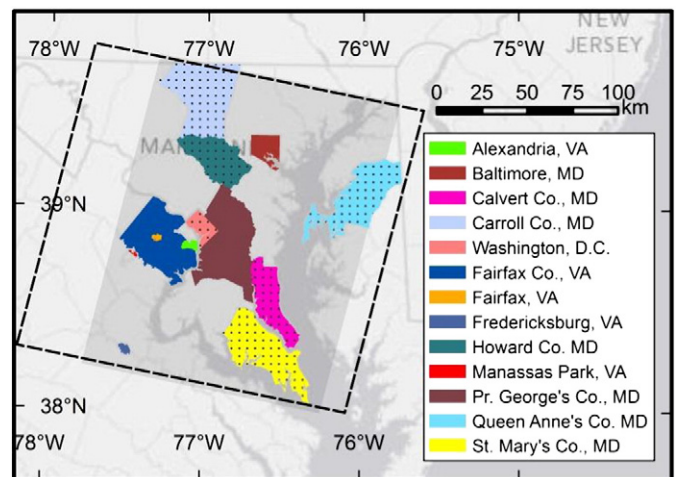


Fig. 1. Study area. Counties labeled are those for which impervious surface reference data were collected. The dotted line represents the nominal WRS-2 boundary, but the shaded region indicates the effective study area, the intersection of all WRS-2 images used.

area. These data were provided by: Calvert and Howard counties, MD for 2006; Carroll and St. Mary’s counties, MD for 2007; and Washington, D.C. and Queen Anne’s County, MD for 2008. Polygons surrounding roads, parking lots, buildings, driveways, and sidewalks using sub-meter resolution imagery were digitized by local municipalities. These data were generalized to a common binary pervious/impervious scheme (including all of the above features as “impervious” and the excluded “background” polygon assumed to be undeveloped, pervious surface), transformed to a common geographic projection, rasterized to (binary) 1-m resolution, and resampled to continuous (percent-cover) scale at Landsat (30-m) resolution. Eighty-five percent of the ISC pixels were used as a training sample for model fitting, and the other 15% were randomly sampled and withheld as a test sample for validation.

2.3.2. Predictor data

Landsat-5 Thematic Mapper (TM) images were selected based on seasonal criteria (Fig. 2). The calendar year was divided into phenological peak and dormant seasons (i.e., “summer”, from DOY 129 to 273 and “winter”, from DOY 1 to 80 and DOY 320 to 366), excluding spring and autumn transitions to avoid inter-annual variation, by inspection of 10-year phenological norms derived from NDVI measurements from the MODerate-resolution Imaging Spectrometer (MODIS) over deciduous forest pixels within the WRS-2 scene (Kim et al., 2011). Within peak and dormant seasons, every Landsat TM image with less than 10% cloud cover estimated by the Automated Cloud Cover Assessment (ACCA) was downloaded from USGS EROS Data Center. Winter images were visually inspected, and those with visible snow cover were removed.

Retained images were processed through the Landsat Ecosystem Disturbance Adaptive Processing System (LEDAPS) (Masek et al., 2006), an implementation of the 6S atmospheric correction codebase

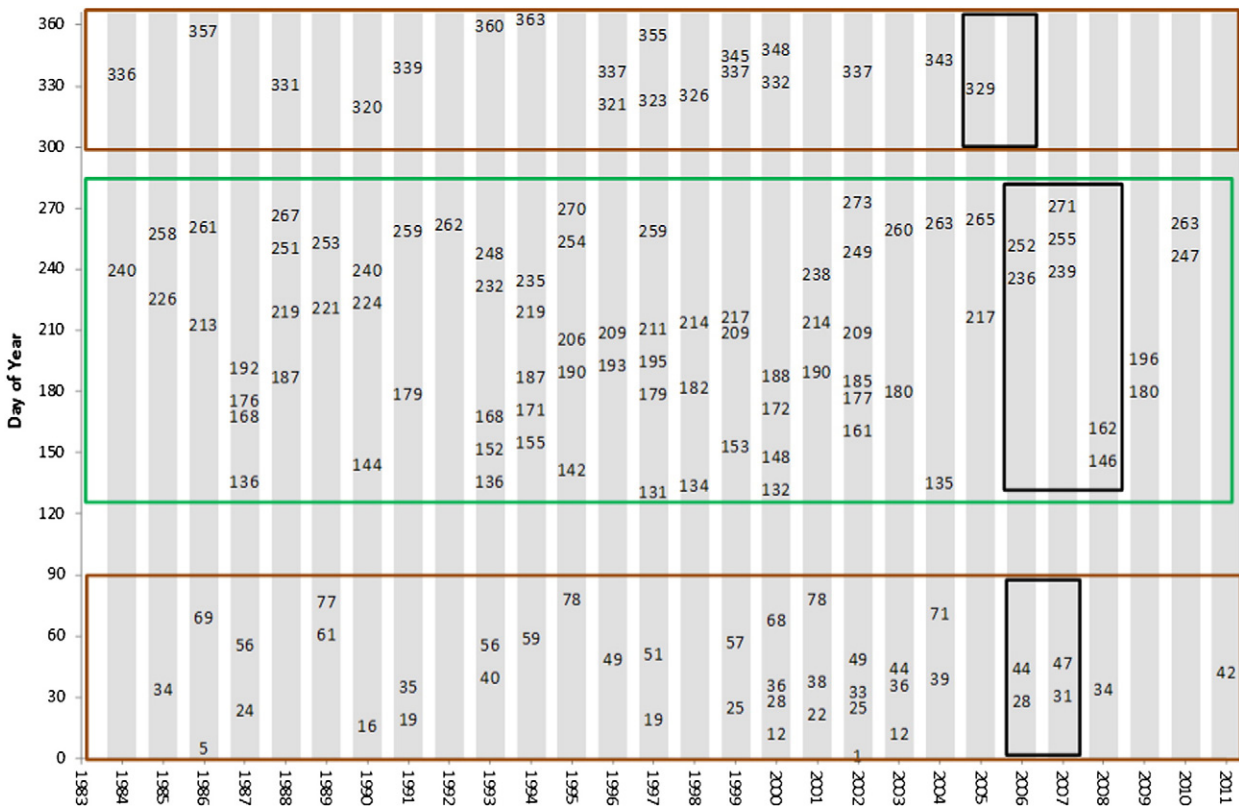
(Vermote & Kotchenova, 2008), to minimize atmospheric effects and retrieve estimates of surface reflectance. Clouds, cloud shadows, and water were masked using methods described by Huang et al. (2010).

Depending on acquisition date, images were composited into either summer or winter predictors in order to minimize residual atmospheric and phenological variation. For winter predictors, the median of each solar-reflective band was calculated from the cloud- and shadow-free pixels of the selected winter images within any year and its adjacent winter months from the years before and after (i.e., DOY 320 to 366 from the previous year and 1 to 80 from the following year), resulting in a single, six-band image of winter medians for each approximately 491-day nominal “year”. Although taking medians of three full years could obscure abrupt changes, this blurring artifact was minimized by shrinking the temporal window to include only the winter months in the preceding and following years that were directly adjacent to the year of interest.

Surface reflectance values were standardized and normalized to remove environmental noise remaining after physical atmospheric correction, e.g., the brightening effect of thin clouds or the darkening effect of their partial shadows (Fig. 3). The bands of each pixel were then standardized to a common dynamic range via:

$$\rho'_{ib} = \frac{\rho_{x,b}}{\max_b(\rho_b)} \tag{1}$$

where ρ_{xi} is the reflectance of band b in pixel i , standardized by dividing by an a priori upper limit to reflectance in that band: blue (0.100), green (0.110), red (0.120), near-infrared (0.225), shortwave-infrared 1 (0.205), shortwave-infrared 2 (0.150). This standardization is commonly employed in ecology for equalizing the contributions of rare and abundant species to indices of community similarity (Legendre



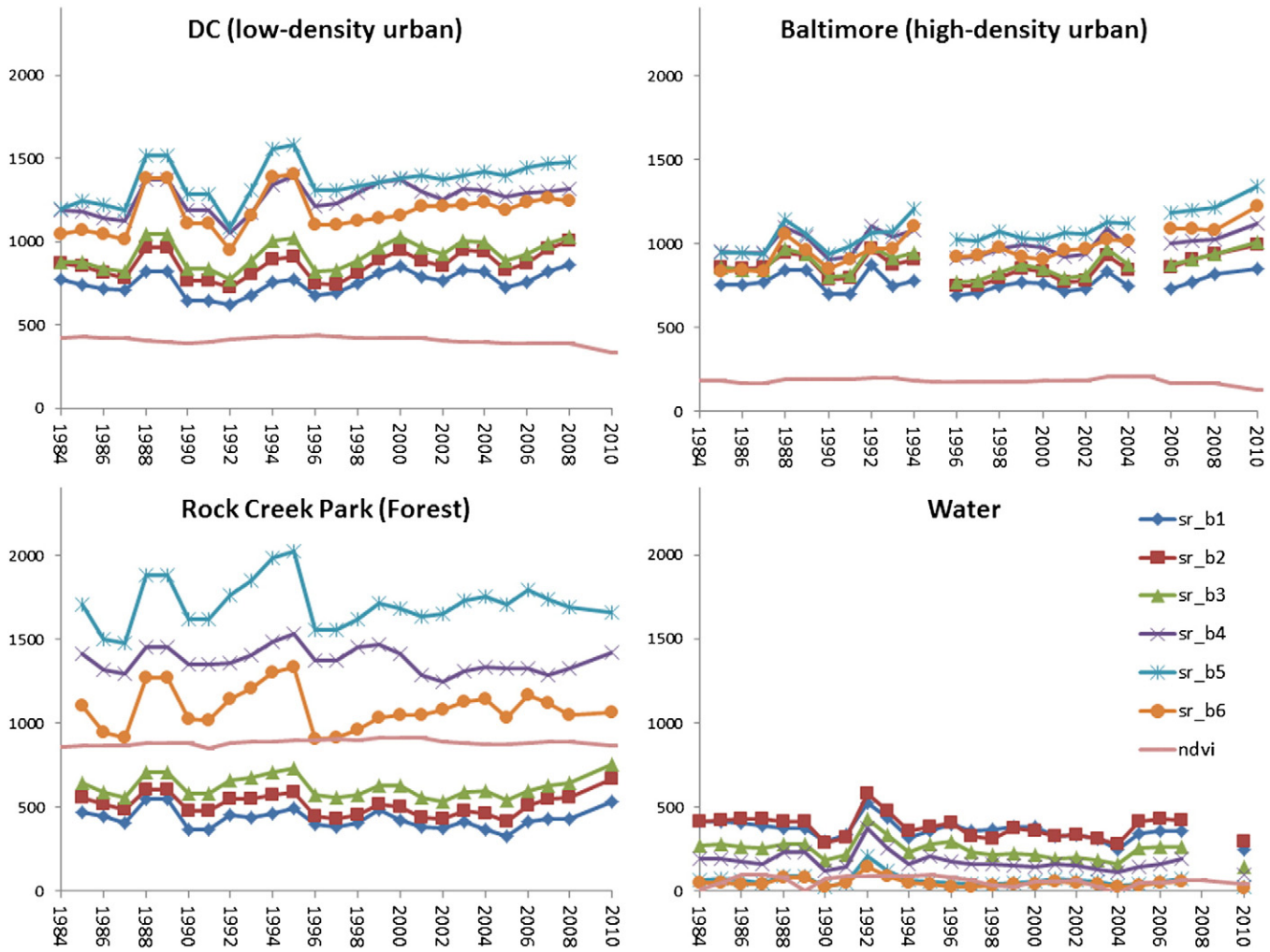


Fig. 3. Winter-median surface reflectance values over time for selected stable pixels of representative land cover types within the study area. Missing values over Baltimore and water are due to clouds. Note the synchronicity of fluctuations between bands in comparison to the stability of NDVI over time (NDVI has been rescaled by a factor of 1000 for comparison.) (For interpretation of the references to color in this figure legend, the reader is referred to the web version of this article.)

& Legendre, 1998). Standardized reflectances were then normalized by dividing by their across-band sum in each pixel:

$$\rho_{i,b}'' = \frac{\rho'_{i,b}}{\sum_i \rho'_{i,b}} \quad (2)$$

This process operated at the pixel level and satisfactorily reduced inter-annual variations that were correlated across all bands (Fig. 4).

The normalized winter medians were augmented with information from the growing season to maximize discrimination between intermittently bare agricultural fields and persistently bare impervious surfaces. The Normalized Difference Vegetation Index (NDVI) was calculated from summer images, and then each summer NDVI pixel was subjected to a three-year (summer) trailing-maximum convolution:

$$sNDVI_t = \max_t^{t+2} (NDVI_t) \quad (3)$$

in which the maximum NDVI value is taken for each pixel in summer images of the nominal year and the two years following. This process consistently minimized year-to-year phenological differences and amplified the difference between vegetated and unvegetated surfaces across urban, suburban, and agricultural land uses (Fig. 5).

2.4. Modeling

Impervious surface layers were overlaid on seasonal Landsat measurements from coincident years, and a joint sample of reference and predictor variables was extracted to generate a multi-year training dataset ($n = 2,178,175$). The training data were used to fit a regression tree (Cubist™; Quinlan, 1993) to infer impervious surface cover from the winter median reflectances and summer maximum NDVI. The fitted model was applied to every year's two-season Landsat data from 1984 to 2010 to retrieve annual estimates of impervious surface cover. Impervious cover of pixels missing reflectance data in one season (e.g., due to cloud cover) was estimated based on available data from the other season.

2.5. Validation

Errors were evaluated relative to the training data by ten-fold cross validation and also to the ~15% withheld (i.e., not included in training) sub-sample of the reference data for model testing ($n = 396,751$). Ten-fold cross validation is a procedure in which the mean value of a selected metric is calculated based on ten random subsets of the original data; the data are split into 10 random sub-sets, a model fit to 90% of the data is validated against each remaining 10% in iteration across the ten subsets, and the mean is

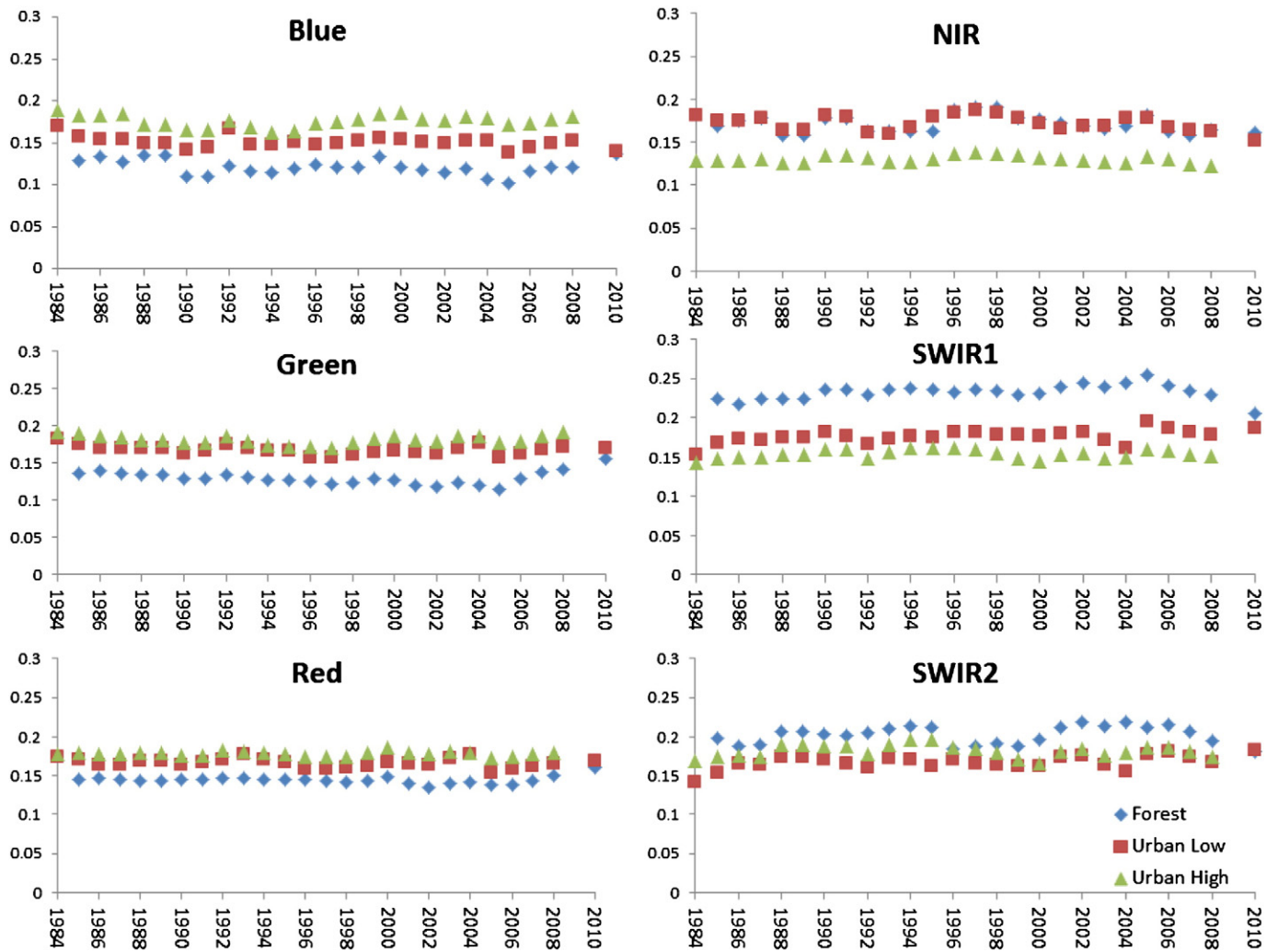


Fig. 4. Standardized and normalized winter-median surface reflectance values over time for forest, high-density urban, and low-density urban pixels. Note the stability of the values compared to the untransformed data in the previous figure. (For interpretation of the references to color in this figure legend, the reader is referred to the web version of this article.)

calculated from the ten sub-sample evaluations. Cross-validation was performed primarily for the purposes of model development, whereas validation based on the withheld sample was used for estimation and characterization of errors. Uncertainty metrics were based on average differences between paired model and reference values, quantified by Mean Bias Error (MBE), Mean Absolute Error (MAE), and Root-Mean-Squared Difference (RMSD):

$$\text{MBE} = \sum_{i=1}^n \frac{M_i - R_i}{n} \quad (4)$$

$$\text{MAE} = \sum_{i=1}^n \frac{|M_i - R_i|}{n} \quad (5)$$

$$\text{RMSD} = \sqrt{\frac{\sum_{i=1}^n (M_i - R_i)^2}{n}} \quad (6)$$

where M_i and R_i are respectively modeled and reference impervious cover values at a location i in a sample of size n .

3. Results

3.1. Model fit and validation

Internal cross-validation of the regression tree estimated an average error (MAE) of $\pm 5.9\%$ cover, with a correlation coefficient between

inferred and observed cover of 0.64. Estimates were constrained to lie within the interval of 0–100% cover, so errors were predominantly positive at low impervious cover and negative at high cover. Results were identical for training and withheld test data, suggesting negligible model over-fitting within the sample relative to the population. All variables were used with approximately equal frequency in terminal-node regressions, but summer-maximum NDVI was by far the most important predictor in terms of usage rate in conditional splits (Table 1). Winter-median blue, SWIR2, and red reflectances were each used in approximately half of tree splits, whereas winter-median SWIR1, green, and NIR reflectances were relatively unimportant in defining tree splits.

Differences between estimated and reference values of percent impervious cover had a strongly peaked distribution centered close to zero (Fig. 6). The average difference between model and reference cover (Mean Bias Error, MBE) was -3.5% , with a median of 0.0. The skew was due to a small mode of large, negative errors located at approximately 100% cover in the reference data, which further inspection revealed to be under-estimation of impervious cover in the shadows of tall buildings – an artifact imposed by the shallow illumination angles of winter images. Another source of under-estimation was the obscuring of roads, sidewalks, and other short-statured structures by trees – an artifact which was partially, but not completely, minimized by using dormant-season images. Over-estimates tended to be small, following an approximately negative-exponential distribution, whereas under-estimates were more normally and widely distributed. MAE of

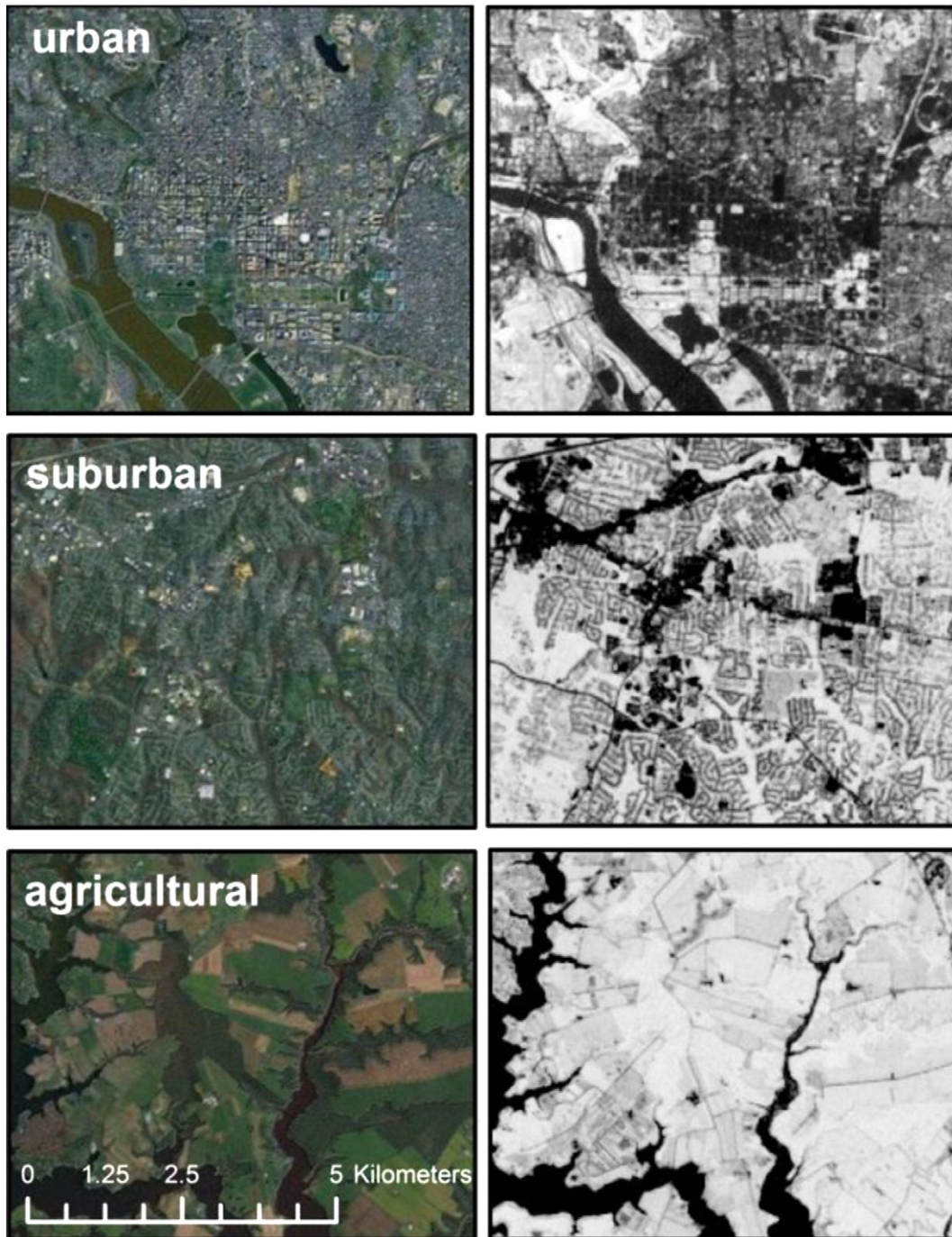


Fig. 5. Demonstration of 3-year, summer-maximum NDVI in urban (Washington, D.C.), suburban (Northern Virginia), and agricultural (Delmarva Peninsula, Maryland) regions.

independent test data was 5.87%, equal to that obtained from cross-validation. RMSD was much higher, 14.46%, corroborating the strong influence of outliers. The correlation coefficient (r) between estimated

Table 1
Cubist™ regression tree summary of predictor variable importance.

Predictor layer	Condition (split) use rate	Terminal-node regression use rate
Summer-maximum NDVI	0.82	0.82
Blue	0.55	0.76
SWIR2	0.54	0.83
Red	0.48	0.73
SWIR1	0.13	0.80
Green	0.11	0.75
NIR	0.05	0.71

and reference impervious cover was 0.64, again likely due to the leverage of outliers on the negative tail of the error distribution.

Although uncertainty increased in proportion to area, local dynamics were captured with high certainty. This local precision is exemplified by the development of FedEx Field, a sports stadium in Landover, Prince George's County, Maryland (Fig. 7). Impervious surfaces that remained constant at or near zero cover values in all three image dates (1993, 2001, and 2010) are black – e.g., the large patches of forest and fields in the western and northeastern portions of the image. Patches that remained at or near complete (100%) impervious cover in all three years – e.g., the numerous large roads and commercial parcels throughout the image – are white. Patches with constant values between 0 and 100% range in various shades of gray – e.g., the curving residential streets, which exhibit an erroneous bluish tint due to the filling in of

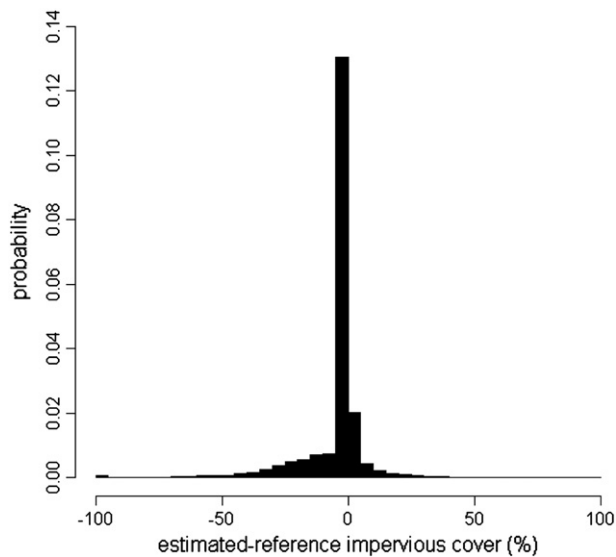


Fig. 6. Distribution of error in estimates of percent impervious surface cover relative to a random 15% sub-sample of reference data withheld for validation. Data are from a pooled sample from several municipalities over three years.

landscape trees over multiple decades. Patches that were developed between 1993 and 2001 and remained so in 2010 are yellow – e.g., FedEx Field, slightly below and right of center in the image, was built in 1997. Note the elliptical patch of zero-impervious cover in the center of the stadium; this is the grass playing field. Patches that were developed between 2001 and 2010 are red – e.g., the commercial–residential development in the northeast corner of the image (Note that development is captured reliably regardless of whether the preceding land cover was forest or herbaceous agriculture.). The cyan patch in the northwest corner of the image is an exceedingly rare class of urban change: impervious surface loss, which can be confirmed as buildings in 1993 and 2001 but bare, disturbed soil in 2010.

3.2. Impervious surface development of the Washington, D.C.–Baltimore, MD region

In 1984, the region had approximately $88,129 \pm 1135$ ha of impervious surface cover – $0.037 \pm 0.0012\%$ of the total area. In 2010, the region's impervious cover had grown to approximately 117,646 ha of impervious surface (4.9% of the total area). The average annual rate of growth was 1135 ± 208 ha/year ($P < 0.0001$) – i.e., approximately 11 km² of new impervious surfaces gained per year over the region. The distribution of impervious surface in 1984 shows the two major cities of the region—Washington, D.C. and Baltimore, MD—as hotspots of impervious cover linked by a suburban corridor served by rail and a number of arterial roads, including Interstate highway I-95, US highway US-29, and Maryland State Route-2 (Fig. 8). Richmond, Virginia lies well to the south, connected to Washington, D.C. by I-95. Annapolis, MD, the state capital, is also visible as a small cluster of impervious surface south of Baltimore and East of Washington, D.C. on the Chesapeake Bay and connected to Washington by US Highway 50 and to Baltimore by I-97, which was completed in 1993. The heavily industrialized Baltimore has a greater density of impervious surface than the more residential cities, Washington and Annapolis, whose principal economies are governance. Several smaller cities and towns are also visible as clusters of impervious surface between Washington and Baltimore, interconnected by a lattice of arterial highways and smaller roads. The Patuxent Wildlife Research Refuge, which is covered predominantly by forests, fields, and natural wetlands, is a large patch of persistent non-impervious cover between 1984 and 2010 within the suburban D.C.–Baltimore corridor. Likewise, agricultural lands are visible as large regions of low impervious cover outside the greater metropolitan

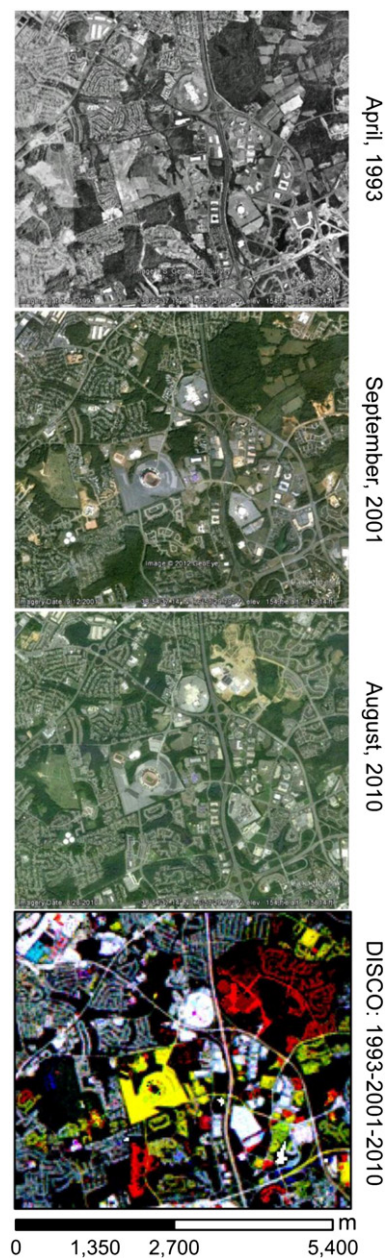


Fig. 7. Development of FedEx Field (Landover, MD) and surrounding neighborhoods. The temporal composite (bottom) shows impervious cover in 1993 in blue, 2001 in green, and 2010 in red. White pixels were impervious in all three dates, and black pixels were non-impervious in all three dates. Pixels that were impervious in both 2001 and 2010 but not in 1993 are displayed in yellow (e.g., FedEx Field, near the center of image), and pixels that were impervious in 1993 and 2001 but not 2010 are in cyan (e.g., demolished building in northwest corner of image). Pixels that were became impervious between 2001 and 2010 are red – e.g., the residential subdivision in the northeast corner of the image.

area (e.g., northwest corner of the study area, southeast of Washington, and east of the Chesapeake Bay).

By 2010, the impervious surface of the small towns between Washington and Baltimore—as well as that of Washington and Baltimore themselves—had intensified and expanded. Infill development is apparent as intensification of increasing imperviousness within the cities. Road widening is also visible, e.g., as an increase in impervious surface percentage of the US-50 roadway. Fragmentation and isolation of natural forest habitat are apparent as increases of impervious surfaces abutting and surrounding the wildlife refuge and other areas.

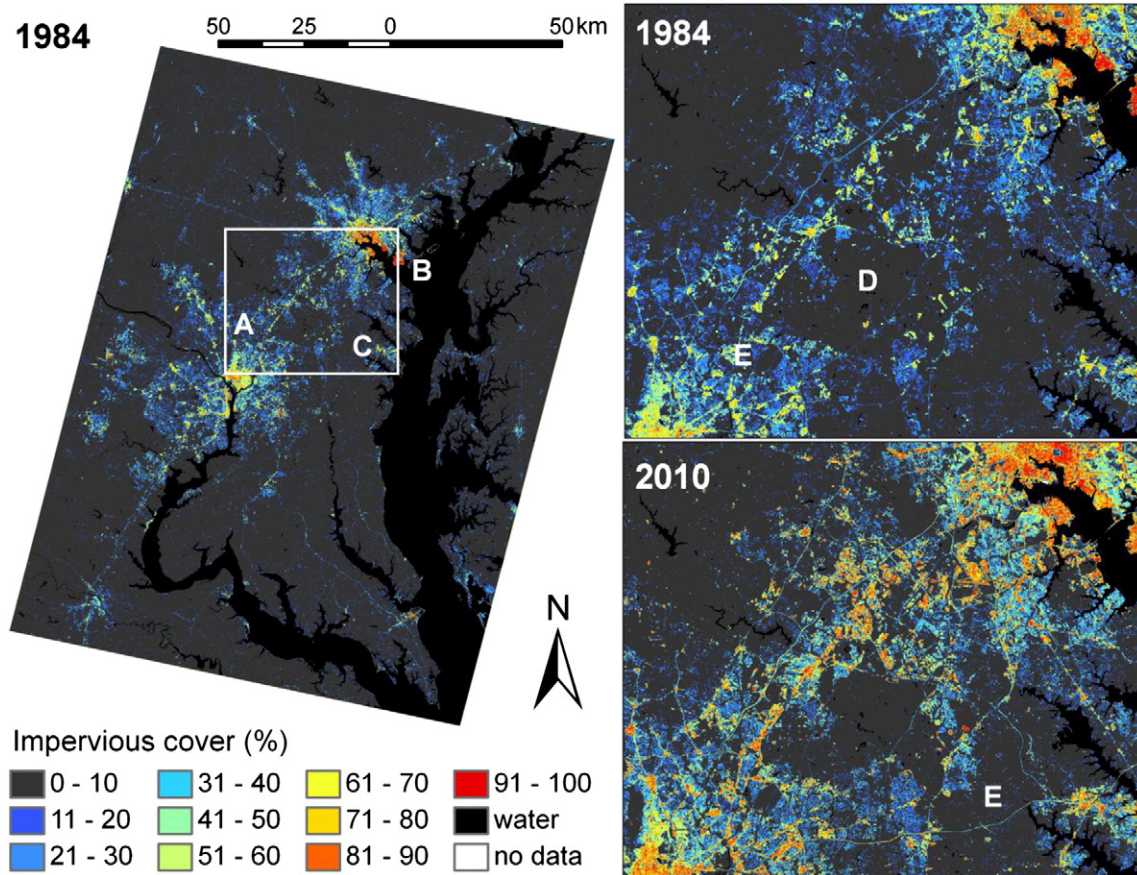


Fig. 8. Impervious surface cover of the study area in 1984, and growth of the D.C.–Baltimore corridor from 1984 to 2010. Points of interest are: (A) Washington, D.C.; (B) Baltimore, Maryland; (C) Annapolis, Maryland; (D) Patuxent Wildlife Research Refuge; and (E) US Highway 50. Note that the data displayed are from years without training data.

Linear growth is observable in several of the region’s municipalities (Fig. 9, Table 2). Fairfax county showed the greatest increase in impervious area, at a rate of 163.91 ± 21.67 ha/year, or $0.16 \pm 0.021\%$ of the county area per year ($p < 0.001$). Calvert county developed much more slowly, at a rate of 11.52 ± 4.56 ha, or $0.02 \pm 0.008\%$, per year ($p = 0.019$). Howard county’s impervious surface cover nearly doubled in area, increasing at a rate of 65.29 ± 7.08 ha ($0.1 \pm 0.01\%$) per year, and that of Prince George’s County, MD increased at a rate of 108.22 ± 24.5 ha ($0.09 \pm 0.02\%$) per year. However, given the small proportion of change over the large areas of the counties, precision was insufficient to consistently observe second-order changes such as acceleration or deceleration. Uncertainty in impervious surface cover increased with area, so the temporal trajectories of the larger counties—e.g., Prince George’s County, MD and Fairfax County, VA—are surrounded by greater noise than are the smaller Howard and Calvert Counties, MD. However, this variation is consistent with overall error estimates.

Although lying in different states and therefore different taxation and zoning policies, Fairfax and Prince George’s counties shared similar growth patterns: low to intermediate fractional cover, high areal cover, and rapid development over the study span — suggesting that their other similarities (e.g., large, suburban, and close to the District of Columbia) have a greater effect on development than local land-use policies. Their large size and large proportion of intermediate cover values also likely led to their relatively large uncertainties.

Cities were proportionally more developed than counties (Fig. 9), with Baltimore, MD, Alexandria, VA, and Washington, D.C. the most developed municipalities in the region. Cities showed great variability in development rates, both among municipalities and within some municipalities over time. In general, impervious surface growth in cities was inversely proportional to existing impervious surface cover. The larger,

more developed cities of Baltimore and Washington, D.C. began with higher proportional coverage and showed very little change over the period of study. In contrast, Manassas Park, VA began with a low proportion of impervious cover (~8%), but accelerated development around 1995, shifting from growth of approximately 4% from 1984 to 1995 (~0.3%/year) to nearly 0.6%/year from 1995 to 2010 (Fig. 9). Although the impervious cover of Fairfax city grew at a slow pace between 1984 and 2010, that of Fairfax County grew much more quickly, indicating exurban, or “sprawl” development. Similarly, Fredericksburg, VA accelerated its rate of development around the same time, shifting from near zero growth from 1984 to 1995 to approximately 0.3% areal increase per year from 1995 to 2010. However, even given the clear growth of small cities such as these, much of Fredericksburg’s development was outside its municipal boundaries (Fig. 10).

4. Discussion

4.1. Urban growth of the Washington, D.C.–Baltimore, MD metropolitan region

The Washington, D.C. metropolitan area and the greater Chesapeake Bay watershed have received much attention due to their rapid development and ecological importance. Masek et al. (2000) used differences in NDVI in two intervals (i.e., between three image dates) from 1973 to 1996 to detect changes in urban cover in the Washington, D.C. metropolitan area. Jantz et al. (2005) assessed the loss of resource lands in the broader Chesapeake Bay watershed between 1990 and 2000 by overlaying a discretized map of impervious cover change from 1990 and 2000 on land cover maps from circa 1990. Suarez-Rubio et al. (2012) assessed exurban development in northern Virginia

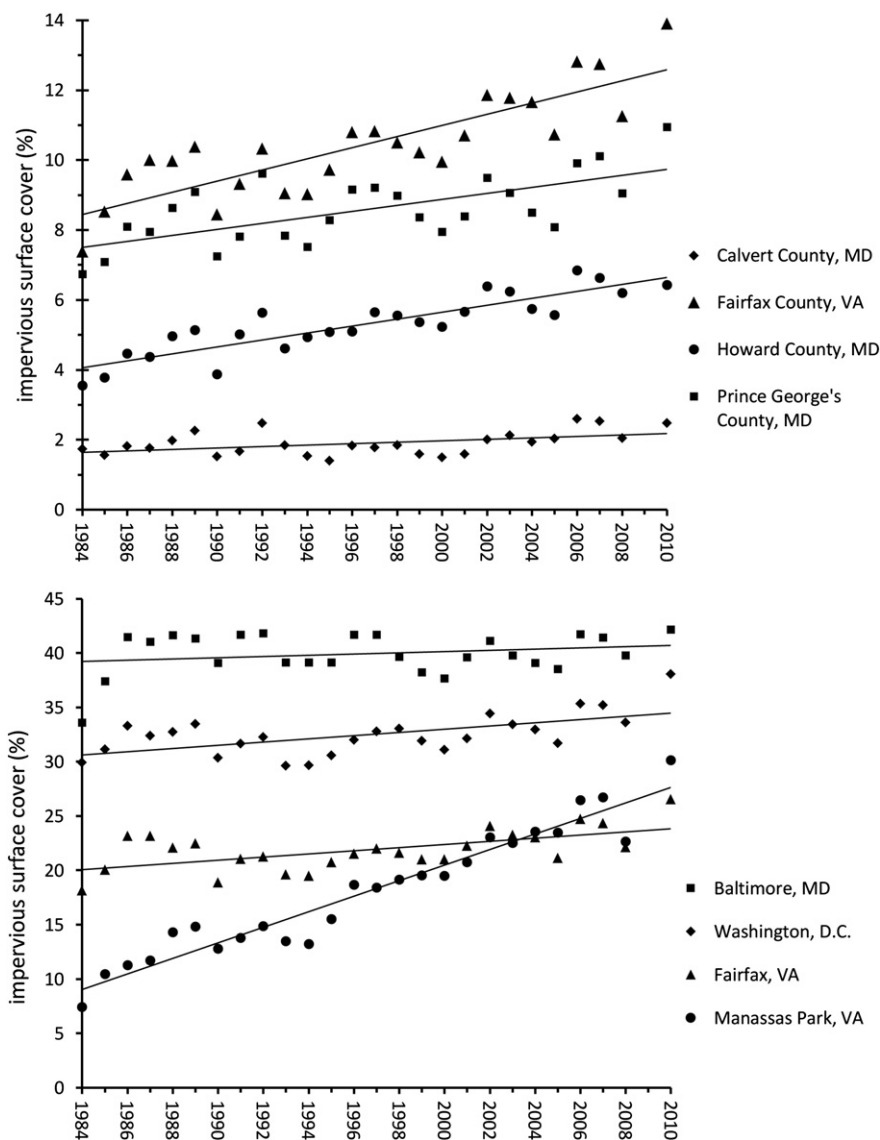


Fig. 9. Estimated change in impervious surface coverage of selected counties (top) and cities (bottom) from 1984 to 2010. No impervious cover map was possible for 2009, due to lack of winter data availability from major snowstorms in 2009 and early 2010. Solid lines represent linear models for each municipality.

and western Maryland between categorical maps from 1986, 1993, 2000, and 2009.

The areas of interest of these studies all differ, and each study responded to the uncertainty of its urban cover estimates by coarsening the thematic resolution to broad categories. However, some similarities are evident despite the differences in spatial and thematic scale. Overall, urban land cover increased at a rapid and accelerating pace in the region, with growth concentrated at the expanding fringes of existing urban clusters. Growth in counties neighboring cities exceeded that of outlying counties as well as the cities themselves, reflecting a predominance of low-density development. Development patterns varied across jurisdictions, with some counties adopting clustered patterns (e.g., Montgomery County, MD) and others adopting more dispersed patterns of sprawl (e.g., Fairfax and Loudoun counties, VA).

Although all these studies are in agreement over the general spatial patterns and temporal trajectories of urbanization in the region, one important difference is evident between previous studies and our own. Masek et al. (2000) found an increase in built-up area of 22 km²/year, Jantz et al. (2005) found a 41% increase in impervious surface area over the entire watershed (most of which is less developed than the Washington–Baltimore area), and Suarez-Rubio et al.

(2012) found an increase of 6.1%/year growth in exurban development alone. In contrast, our estimate based on per-pixel percentages of impervious cover (~11 km²/year) is much more conservative than any of these findings based on categorized data. Because urbanization in the region is dominated by sparse development, our estimate, which is based upon data of higher thematic resolution, should be considered a refinement of these earlier estimates.

4.2. Long-term retrieval of impervious surface cover from the Landsat archive

In a recent review of remote sensing methods for estimating impervious surface cover, Weng (2012) called for more research in the change and evolution of impervious surfaces over time. The review focused on novel machine learning algorithms and new data sources, concluding that high-resolution, SAR, LiDAR, and other new image products can increase accuracy of maps of present and recent conditions. However, these new datasets do not have the spatial coverage or temporal scale needed to monitor urbanization over the long term.

The Landsat series of sensors, spanning over thirty years of Earth's dynamic recent history, is unique in its ability to support retrieval of

Table 2

Summary of regression coefficients and fit of linear regression of impervious surface area (ha) and cover (percent of municipal area) over time (years) from 1984 to 2010, excluding 2009 ($n = 26$, $d.f. = 24$) for selected counties and cities. Cities and counties in bold font are mentioned in text.

Municipality	Intercept ^a			Slope			R ²
	ha (S.E.)	% (S.E.)	P (> t)	ha/year (S.E.)	%/year (S.E.)	P (> t)	
Washington	4934 (96)	30.63 (0.59)	0.000	23.9 (6.5)	0.15 (3.65)	0.001	0.357
Anne Arundel County	7365 (307)	6.83 (0.29)	0.000	75.5 (21.0)	0.070 (0.02)	0.001	0.350
Baltimore	8274 (153)	39.25 (0.73)	0.000	11.7 (10.5)	0.06 (0.05)	0.275	0.049
Calvert County	933 (67)	1.65 (0.12)	0.000	11.5 (4.6)	0.02 (0.01)	0.019	0.210
Charles County	1861 (143)	1.56 (0.12)	0.000	32.7 (9.8)	0.03 (0.01)	0.003	0.318
Howard County	2666 (104)	4.06 (0.16)	0.000	65.3 (7.1)	0.10 (0.01)	0.000	0.780
Montgomery County ^b	7034 (257)	5.46 (0.20)	0.000	91.7 (17.6)	0.07 (0.01)	0.000	0.531
Prince George's County	9485 (359)	7.51 (0.28)	0.000	108.2 (24.5)	0.09 (0.02)	0.000	0.448
St. Mary's County	2163 (139)	2.27 (0.15)	0.000	-1.5 (9.5)	-0.000 (0.01)	0.877	0.001
Arlington	1707 (50)	25.23 (0.74)	0.000	6.0 (3.4)	0.09 (0.05)	0.090	0.115
Alexandria	1288 (32)	32.80 (0.82)	0.000	1.2 (2.2)	0.03 (0.06)	0.586	0.013
Fairfax	330 (10)	20.06 (0.59)	0.000	2.4 (0.6)	0.15 (0.04)	0.001	0.352
Fairfax County	8694 (317)	8.45 (0.31)	0.000	163.9 (21.7)	0.16 (0.02)	0.000	0.704
Falls Church	100 (4)	19.38 (0.76)	0.000	0.7 (0.3)	0.13 (0.05)	0.021	0.203
Fredericksburg	311 (14)	11.39 (0.53)	0.000	8.5 (1.0)	0.31 (0.04)	0.000	0.755
King George County	454 (38)	0.95 (0.08)	0.000	5.9 (2.623)	0.01 (0.01)	0.034	0.174
Manassas	450 (18)	17.38 (0.68)	0.000	11.2 (1.2)	0.43 (0.05)	0.000	0.781
Manassas Park	58 (4)	9.04 (0.59)	0.000	4.6 (0.3)	0.72 (0.04)	0.000	0.930
Stafford County	971 (85)	1.37 (0.12)	0.000	36.8 (5.8)	0.05 (0.01)	0.000	0.629

^a Years are adjusted so that the intercept is estimated at year 1984.

^b Partial coverage in study area.

land cover change records over long time scales (Goward et al., 2006; Gutman & Masek, 2012). However, fitting individual models for each place and time is simply too inefficient (and demanding of often non-existent archival reference data) for long-term retrievals. Alternatively, extrapolation of robust models based on physically or statistically normalized imagery is a much more practical approach for extracting information from the full spatial and temporal extent of the Landsat archive. Whereas most algorithm development to date has focused on maximizing accuracy in relatively few points in time so that traditional change detection methods may be employed, our regression-based approach allowed continuous-field estimation and statistical inference using nearly every year in a twenty-seven year span.

Several factors enable use of Landsat data for long-term monitoring of impervious surface dynamics. Of primary importance is the United States' open-access data policy begun in 2009. Without inexpensive (or free) data, impervious and other land cover mapping efforts would not have access to sufficient data volumes to fill cloud gaps or remove phenological and atmospheric noise by high-volume image compositing. Secondarily, reliable radiometric calibration, atmospheric correction, and phenological selection are required for consistent extrapolation of models to locations and times not sampled by reference data (Masek et al., 2006). Also, recent development of image compositing techniques for Landsat data (e.g., Huang et al., 2009a, 2009b; Roy et al., 2010) are necessary to dampen remnant noise and identify the spectral and temporal signatures of impervious or other surface materials.

The potential temporal domain of the specific method demonstrated here is the era of Landsat-5 and Landsat-7 (i.e., from 1984 to the present). With wider uncertainties, extension back to 1972 might be possible where sufficient Multi-Spectral Scanner (MSS) data are available (and similarly forward to newer sensors), although methods must be developed to extrapolate models between sensors. Due to the method's reliance on the phenological discrimination of impervious surfaces, the potential spatial domain of the method is confined to humid temperate biomes, where rapid vegetation regrowth distinguishes intermittently bare soil from persistently bare urban surfaces. The approach is less likely to provide accuracy in arid, alpine, or otherwise sparsely vegetated regions. Ultimately, however, this—and any other—empirical method requires high-quality reference data with adequate sampling over space and time to represent the range of conditions within the domain

of extrapolation. For this, there is no better source of information than the municipalities who record impervious surface coverage for the purposes of storm-water management and taxation.

The primary impediment to observing rapid changes in our time series was imprecision of impervious cover estimates in the temporal dimension. Although the pattern of cover was consistent across space in any year, temporal trajectories of cover in any selected region exhibited oscillations that cannot plausibly be attributed to real change (Fig. 9). These errors could be reduced statistically, by increasing sampling of training data in the temporal domain, removing noise from the estimates and increasing model variance. However, given the consistency of the oscillation, there is likely a physical explanation for the phenomenon. Landsat-5 orbited on a cycle repeating approximately every six years (not including adjustments), similar to the frequency of the observed oscillation. This suggests the possibility of Bidirectional Distribution Function (BRDF) effects. BRDF effects have been observed in Landsat across space (Danaher et al., 2001), but only recently have the data become sufficient to detect BRDF effects over time. To ensure the precision of Landsat measurements in time as well as space, this is an area of research which should be explored.

Remaining uncertainty notwithstanding, the multi-temporal accuracies yielded by temporal compositing in this study are comparable to those reported for static and coarse time-series maps in similar environments (Jiang et al., 2009; Yang et al., 2003, 2009). However, some known challenges still remain. These include: generalization of rules for phenological selection and compositing of images, analysis and prediction of errors in locations and years not sampled with reference data, and development of change-detection methodologies that make use of both continuous-scale data and estimates of uncertainty. Similar issues challenge efforts to monitor forest cover (e.g., Hansen et al., 2010; Huang et al., 2009a, 2009b; Kennedy et al., 2010; Sexton et al., 2013; Townshend et al., 2012), and so there is much room for mutual learning and advancement between these closely related fields of study.

4.3. A call for long-term, consistent records of land-cover change

Long-term records of impervious surface cover have great potential for application among urban growth modelers and managers of policies governing land-use change, as well as ecologists, hydrologists, and economists studying the effects of urbanization on physical, biological, and socio-economic systems. Rich in theory but relatively poor in

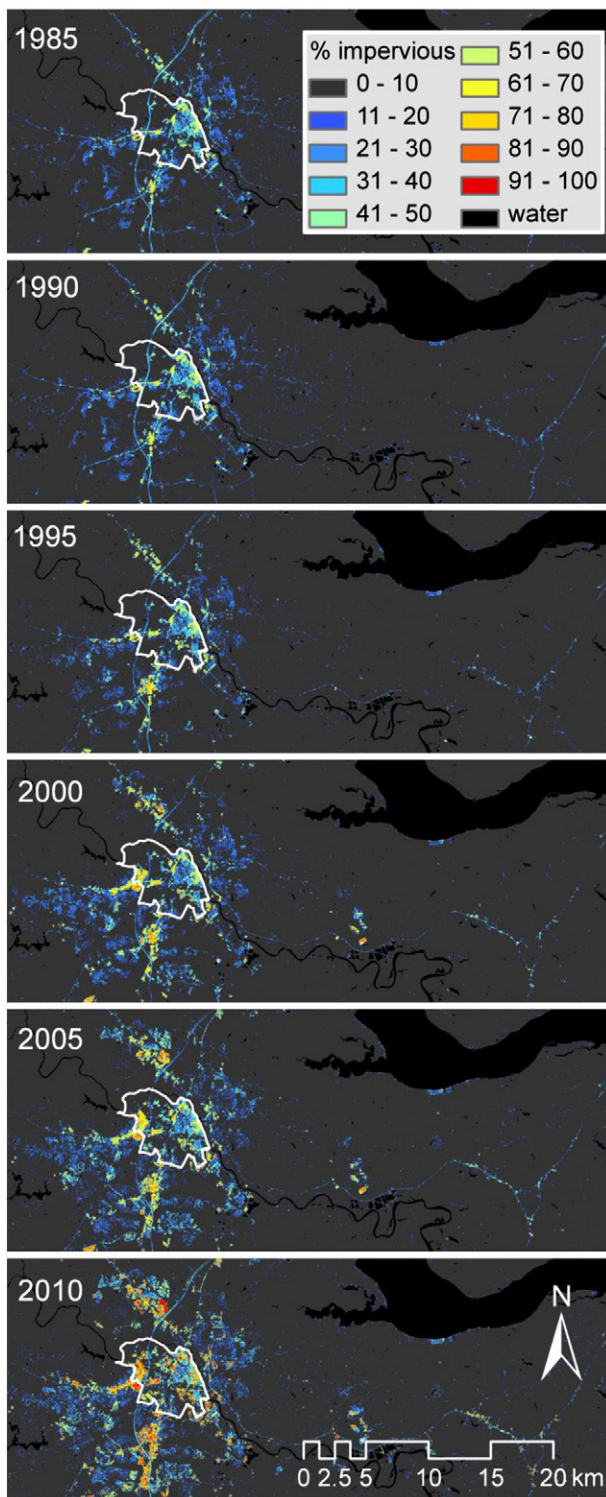


Fig. 10. Impervious surface development of Fredericksburg, VA from 1985 to 2010. The circa-2010 municipal boundary is outlined in white. Note that reference data were not available either within the spatial extent or any of the years presented.

data, each of these groups is currently forced to base inference on uni-temporal, or at best coarsely multi-temporal, databases. In the social sciences, inferences are commonly drawn by comparing a few, intensively studied case studies representing different scenarios (Turner et al., 2007), and similar limitations underlie the “space-for-time substitution” commonly employed in ecology (Pickett, 1989) and “paired

watershed” studies in hydrology. Although recent studies based on multi-temporal landcover maps have shown accelerating rates and shifting patterns of development (e.g., Whitehurst et al., 2009; Yin et al., 2011)—patterns that require at least three observations in time—there are currently no consistent long-term records of land cover to support more powerful inferential approaches.

Efforts to produce the needed datasets, primarily in the area of forest-cover change, are now underway (Cohen et al., 2010; Huang et al., 2009a, 2009b; Kennedy et al., 2010). As these data improve, their primary use will likely continue to be for simple inventories of land cover change, but their denser (i.e., ~annual) temporal sampling will increase scientists' ability to observe the complexities of coupled human–natural systems. This will certainly precipitate more sophisticated socio-economic and ecological models, tighter correlation with other spatio-temporal datasets, and ultimately greater understanding and management of coupled human–natural systems. Already, a growing number of social scientists, ecologists, and physicists are coordinating their efforts to better understand these systems (Daily & Matson, 2008), and it is the responsibility of the remote sensing community to provide them with the long-term, consistent records needed for progress.

5. Conclusion

We have developed a method for retrieving retrospective continuous fields of impervious surface cover at 30-m spatial resolution and annual interval from the Landsat-5 archive, from approximately 1984 to 2010. Our results depict the heterogeneous and nonlinear growth of impervious surfaces among the municipalities of the Washington, D.C.–Baltimore, MD metropolitan region, corroborating and refining the spatial, temporal, and thematic resolution of well-known patterns of urban growth and development. Technically, our results demonstrate that robust estimation and long-term retrieval of impervious cover in humid–temperate (i.e., seasonally vegetated) regions is possible using multi-temporal, multi-spectral (i.e., Landsat-class) data. Of critical importance is maintaining the representativeness of the training sample over space and time, which requires knowledge of vegetation seasonality and recovery from disturbance. Practically, the long-term, high-resolution datasets retrieved by this method enable change detection at arbitrary temporal intervals, as well as observation of long-term acceleration of land-use change. They will thus be of great use to ecologists, hydrologists, and social scientists studying human–environment interactions in urbanizing ecosystems.

Acknowledgments

Primary funding was provided by the Maryland Sea Grant Program, with additional support from the NASA MEASUREs Program. Landsat data was acquired from the USGS EROS Data Center, and reference impervious surface data were provided by: Calvert County, MD Department of Planning & Zoning; Carroll County Government Office of Technology Services; Howard County, MD Government; Queen Anne's County Department of Planning and Zoning; and the Washington, D.C. Office of the Chief Technology Officer. All image processing and analysis were performed at the Global Land Cover Facility, University of Maryland.

References

- Cohen, W. B., Yang, Z., & Kennedy, R. (2010). Detecting trends in forest disturbance and recovery using yearly Landsat time series: 2. TimeSync – Tools for calibration and validation. *Remote Sensing of Environment*, 114(12), 2911–2924.
- Daily, G. C., & Matson, P. A. (2008). Ecosystem services: From theory to implementation. *Proceedings of the National Academy of Sciences*, 105(28), 9455–9456.
- Danaher, T., Wu, X., & Campbell, N. (2001). Bi-directional reflectance distribution function approaches to radiometric calibration of Landsat ETM+ imagery. *Proceedings of the IEEE Geoscience and Remote Sensing Symposium (IGARSS)* (pp. 7031–7034).

- Davis, K. (1945). The world demographic transition. *The Annals of the American Academy of Political and Social Science*, 237(1), 1–11.
- Friedl, M., McIver, D., Hodges, J. C., Zhang, X., Muchoney, D., Strahler, A., et al. (2002). Global land cover mapping from MODIS: Algorithms and early results. *Remote Sensing of Environment*, 83(1–2), 287–302.
- Goetz, S. J., Wright, R. K., Smith, A. J., Zinecker, E., & Schaub, E. (2003). IKONOS imagery for resource management: Tree cover, impervious surfaces, and riparian buffer analyses in the mid-Atlantic region. *Remote Sensing of Environment*, 88(1–2), 195–208.
- Goward, S., Arvidson, T., Williams, D., Faundeen, J., Irons, J., & Franks, S. (2006). Historical record of landsat global coverage: Mission operations, NSLRSDA, and international cooperator stations. *Photogrammetric Engineering and Remote Sensing*, 72(10), 1155–1169.
- Gutman, G., & Masek, J. G. (2012). Long-term time series of the Earth's land-surface observations from space. *International Journal of Remote Sensing*, 33(15), 4700–4719.
- Hansen, M. C., Defries, R. S., Townshend, J. R. G., & Sohlberg, R. (2000). Global land cover classification at 1 km spatial resolution using a classification tree approach. *International Journal of Remote Sensing*, 21(6–7), 1331–1364.
- Hansen, M. C., Stehman, S. V., & Potapov, P. V. (2010). Quantification of global gross forest cover loss. *Proceedings of the National Academy of Sciences*, 107(19), 8650–8655.
- Hodgson, M. E., Jensen, J. R., Tullis, J. A., Riordan, K. D., & Archer, C. M. (1999). Synergistic use of LiDAR and color aerial photography for mapping urban parcel imperviousness. *Photogrammetric Engineering and Remote Sensing*, 29(203), 973–980.
- Homer, C., Huang, C., Yang, L., Wylie, B., & Coan, M. (2004). Development of a 2001 national land-cover database for the United States. *Photogrammetric Engineering and Remote Sensing*, 70(7), 829–840.
- Huang, C., Goward, S., Masek, J., Gao, F., Vermote, E., Thomas, N., et al. (2009a). Development of time series stacks of Landsat images for reconstructing forest disturbance history. *International Journal of Digital Earth*, 2(3), 195–218.
- Huang, C., Goward, S. N., Schleeweis, K., Thomas, N., Masek, J. G., & Zhu, Z. (2009b). Dynamics of national forests assessed using the Landsat record: Case studies in eastern United States. *Remote Sensing of Environment*, 113(7), 1430–1442.
- Huang, C., Thomas, N., Goward, S. N., Masek, J. G., Zhu, Z., Townshend, J. R. G., et al. (2010). Automated masking of cloud and cloud shadow for forest change analysis using Landsat images. *International Journal of Remote Sensing*, 31(20), 5449–5464.
- Jantz, P., Goetz, S., & Jantz, C. (2005). Urbanization and the loss of resource lands in the Chesapeake Bay watershed. *Environmental Management*, 36(6), 808–825.
- Jensen, J. R., & Cowen, D. C. (1999). Remote sensing of urban/suburban infrastructure and socio-economic attributes. *Photogrammetric Engineering and Remote Sensing*, 65(5), 611–622.
- Jiang, L., Liao, M., Lin, H., & Yang, L. (2009). Synergistic use of optical and InSAR data for urban impervious surface mapping: A case study in Hong Kong. *International Journal of Remote Sensing*, 30(11), 2781–2796.
- Kennedy, R. E., Yang, Z., & Cohen, W. B. (2010). Detecting trends in forest disturbance and recovery using yearly Landsat time series: 1. LandTrendr — Temporal segmentation algorithms. *Remote Sensing of Environment*, 114(12), 2897–2910.
- Kim, D.-H., Narasimhan, R., Sexton, J. O. S., Huang, C., & Townshend, J. R. (2011). Methodology to select phenologically suitable Landsat scenes for forest change detection. *International Geoscience and Remote Sensing Symposium (IGARSS)* (pp. 2613–2616).
- Lambin, E. F., Geist, H. J., & Lepers, E. (2003). Dynamics of land-use and land-cover change in tropical regions. *Annual Review of Environment and Resources*, 28, 205–241.
- Legendre, P., & Legendre, L. (1998). *Numerical ecology* (2nd ed.). Amsterdam: Elsevier BV.
- Loveland, T. R., Reed, B. C., Brown, J. F., Ohlen, D. O., Zhu, Z., Yang, L., et al. (2000). Development of a global land cover characteristics database and IGBP DISCover from 1 km AVHRR data. *International Journal of Remote Sensing*, 21(6–7), 1303–1330.
- Lunetta, R. S., Johnson, D. M., Lyon, J. G., & Crotwell, J. (2004). Impacts of imagery temporal frequency on land-cover change detection monitoring. *Remote Sensing of Environment*, 89, 444–454.
- Maryland State Archives (2011). Maryland at a glance. Accessed February 22, 2012. <http://2010.census.gov/2010census/data/apportionment-pop-text.php>
- Masek, J. G., Lindsay, F. E., & Goward, S. N. (2000). Dynamics of urban growth in the Washington, D.C. metropolitan area, 1973–1996, from Landsat observations. *International Journal of Remote Sensing*, 21(18), 3473–3486.
- Masek, J. G., Vermote, E. F., Saleous, N. E., Wolfe, R., Hall, F. G., Huemmrich, K. F., et al. (2006). A Landsat surface reflectance dataset for North America, 1990–2000. *IEEE Geoscience and Remote Sensing Letters*, 3(1), 68–72.
- Menke, S. B., Guénard, B., Sexton, J. O., Weiser, M. D., Dunn, R. R., & Silverman, J. (2010). Urban areas may serve as habitat and corridors for dry-adapted, heat tolerant species: An example from ants. *Urban Ecosystems*, 14, 135–163.
- Oke, T. (2006). The energetic basis of the urban heat island. *Quarterly Journal of the Royal Meteorological Society*, 108(455), 1–24.
- Pickett, S. T. A. (1989). Space-for-time substitution as an alternative to long-term studies. In G. E. Likens (Ed.), *Long-term studies in ecology: Approaches and alternatives* (pp. 110–135). New York: Springer-Verlag.
- Potere, D., Schneider, A., Angel, S., & Civco, L. (2009). Mapping urban areas on a global scale: Which of the eight maps now available is more accurate? *International Journal of Remote Sensing*, 30, 37–41.
- Quinlan, J. R. (1993). *C4.5: Programs for machine learning*. San Francisco, CA: Morgan Kaufmann.
- Roy, D. P., Ju, J., Kline, K., Scaramuzza, P. L., Kovalsky, V., Hansen, M., et al. (2010). Web-enabled Landsat Data (WELD): Landsat ETM+ composited mosaics of the conterminous United States. *Remote Sensing of Environment*, 114(1), 35–49.
- Schneider, A., Friedl, M. A., & Potere, D. (2009). A new map of global urban extent from MODIS satellite data. *Environmental Research Letters*, 4(4) (044003 (11 pp.)).
- Sexton, J. O., Urban, D. L., Donohue, M. J., & Song, C. (2013). Long-term land cover dynamics by multi-temporal classification across the Landsat-5 record. *Remote Sensing of Environment*, 128, 246–258.
- Small, C., Pozzi, F., & Elvidge, C. (2005). Spatial analysis of global urban extent from DMS-OLS night lights. *Remote Sensing of Environment*, 96(3–4), 277–291.
- Suarez-Rubio, M., Lookingbill, T. R., & Elmore, A. J. (2012). Exurban development derived from Landsat from 1986 to 2009 surrounding the District of Columbia, USA. *Remote Sensing of Environment*, 124, 360–370.
- Taubenböck, H., Esch, T., Felber, A., Wiesner, M., Roth, A., & Dech, S. (2012). Monitoring urbanization in mega cities from space. *Remote Sensing of Environment*, 117, 162–176.
- Townshend, J. R., Masek, J. G., Huang, C., Vermote, E. F., Gao, F., Channan, S., Sexton, J. O., Feng, M., Narasimhan, R., Kim, D.-H., Song, K., Song, D., Song, X.-P., Noojipady, P., Tan, B., Hansen, M. C., Li, M., & Wolfe, R. E. (2012). Global characterization and monitoring of forest cover using Landsat data: Opportunities... and challenges. *International Journal of Digital Earth*, 5, 373–397.
- Thomas, N., Hendrix, C., & Congalton, R. G. (2003). A comparison of urban mapping methods using high-resolution digital imagery. *Photogrammetric Engineering and Remote Sensing*, 69(9), 963–972.
- Turner, B. L., Lambin, E. F., & Reenberg, A. (2007). The emergence of land change science for global environmental change and sustainability. *Proceedings of the National Academy of Sciences of the United States of America*, 104(52), 20666–20671.
- UNFPA (United Nations Population Fund) (2011). State of world population in 2011. <http://foweb.unfpa.org/SWP2011/reports/EN-SWOP2011-FINAL.pdf>
- accessed. US Census Bureau (2012). Resident population data. Accessed February 22, 2012. <http://2010.census.gov/2010census/data/apportionment-pop-text.php>
- Vermote, E. F., & Kotchenova, S. (2008). Atmospheric correction for the monitoring of land surfaces. *Journal of Geophysical Research*, 113(D23), D23S90.
- Walsh, C. J., Roy, A. H., Feminella, J. W., Cottingham, P. D., Groffman, P. M., & Morgan, R. P., II (2005). The urban stream syndrome: Current knowledge and the search for a cure. *Journal of the North American Benthological Society*, 24, 706–723.
- Weng, Q. (2012). Remote sensing of impervious surfaces in the urban areas: Requirements, methods, and trends. *Remote Sensing of Environment*, 117, 34–49.
- Westervelt, J., BenDor, T., & Sexton, J. (2011). A technique for rapidly forecasting regional urban growth. *Environment and Planning B: Planning and Design*, 38(1), 61–81.
- Whitehurst, A. S., Sexton, J. O., & Dollar, L. (2009). Land cover change in western Madagascar's dry deciduous forests: A comparison of forest changes in and around Kirindy Mite National Park. *Oryx*, 43, 275–283.
- Yang, L., Huang, C., Homer, C. G., Wylie, B. K., & Coan, M. J. (2003). An approach for mapping large-area impervious surfaces: Synergistic use of Landsat-7 ETM+ and high spatial resolution imagery. *Canadian Journal of Remote Sensing*, 29(2), 230–240.
- Yang, L., Jiang, L., & Liao, M. (2009). Quantifying sub-pixel urban impervious surface through fusion of optical and InSAR imagery. *GIScience and Remote Sensing*, 46, 161–171.
- Yin, J., Yin, Z., Zhong, H., Xu, S., Hu, X., Wang, J., et al. (2011). Monitoring urban expansion and land use/land cover changes of Shanghai metropolitan area during the transitional economy (1979–2009) in China. *Environmental Monitoring and Assessment*, 177(1), 609–621.